

Off-the-grid compressive sensing for broken-rotor-bar fault detection in squirrel-cage induction motors

Liu, D.; Lu, D.

TR2015-096 September 2015

Abstract

In this paper, we propose an off-the-grid compressive sensing based method to detect broken-bar fault in squirrel-cage induction motors. To validate our method, we first build a dynamic model of squirrel-cage induction motor using multi-loop equivalent circuit to simulate motor current under fault conditions. We then develop an off-the-grid compressive sensing algorithm to extract the fault characteristic frequency from the simulated motor current by solving an atomic norm minimization problem. Comparing to other fault detection methods via motor current signature analysis, our method yields high resolution in extracting low-magnitude fault characteristic frequency with only 0.7 second measurements. Simulation results validate our proposed method.

2015 IFAC Symposium on Fault Detection, Supervision and Safety for Technical Processes (SAFEPROCESS)

This work may not be copied or reproduced in whole or in part for any commercial purpose. Permission to copy in whole or in part without payment of fee is granted for nonprofit educational and research purposes provided that all such whole or partial copies include the following: a notice that such copying is by permission of Mitsubishi Electric Research Laboratories, Inc.; an acknowledgment of the authors and individual contributions to the work; and all applicable portions of the copyright notice. Copying, reproduction, or republishing for any other purpose shall require a license with payment of fee to Mitsubishi Electric Research Laboratories, Inc. All rights reserved.

Off-the-Grid Compressive Sensing for Broken-Rotor-Bar Fault Detection in Squirrel-Cage Induction Motors

Dehong Liu * Dingguo Lu **,1

* *Mitsubishi Electric Research Laboratories, Cambridge, MA 02139
USA (e-mail: liudh@merl.com)*

** *University of Nebraska-Lincoln, Lincoln, NE 68588, USA (email:
stan1860@huskers.unl.edu)*

Abstract: In this paper, we propose an off-the-grid compressive sensing based method to detect broken-bar fault in squirrel-cage induction motors. To validate our method, we first build a dynamic model of squirrel-cage induction motor using multi-loop equivalent circuit to simulate motor current under fault conditions. We then develop an off-the-grid compressive sensing algorithm to extract the fault characteristic frequency from the simulated motor current by solving an atomic norm minimization problem. Comparing to other fault detection methods via motor current signature analysis, our method yields high resolution in extracting low-magnitude fault characteristic frequency with only 0.7 second measurements. Simulation results validate our proposed method.

Keywords: Fault detection, broken bar, squirrel-cage induction motor, compressive sensing

1. INTRODUCTION

The squirrel-cage induction motors suffer from a variety of mechanical and electrical faults, of which about 10% are related to broken-rotor-bar (BRB) fault Zhang et al. (2011). The BRB fault can be caused by either imperfections in the manufacturing process, or non-smooth operations such as direct-on-line starting duty cycles and pulsating mechanical loads. Although the BRB fault generally does not lead to instant failures to the induction motors, it causes serious secondary effects, such as excessive vibrations, poor starting performance, and torque fluctuation, *etc.* Even worse, the broken part may hit stator windings at high velocity, causing catastrophic failures on winding insulation. Therefore, it is of great importance to detect the BRB fault in time so as to reduce the cost of maintenance and repair Santos et al. (2006).

In order to detect the BRB fault, signatures are extracted from motor current, air-gap flux, torque, and vibration, *etc.* for further analysis. Among these fault signatures, motor current signature is gaining more attention for its non-invasiveness and low cost. When there exists a BRB fault in the squirrel-cage induction motor, the rotor operates asymmetrically, inducing extra frequency components $f_{sb} = (1 \pm 2\kappa s)f_s$ in the stator current Filippetti et al. (1998), where s is the speed slip, typically ranges from 0.005 to 0.05 under steady operating condition; f_s is the power supply frequency; and $\kappa = 1, 2, 3, \dots$ is the harmonic frequency index. Among these extra components, the $(1 - 2s)f_s$ component is the strongest one and typically treated as the indicator of a BRB fault. Thus frequency $(1 - 2s)f_s$

is also termed the characteristic frequency. BRB fault detection via motor current signature analysis (MCSA) is basically detecting the characteristic frequency component $(1 - 2s)f_s$.

However, it is challenging to detect the characteristic component due to the following factors. First, the magnitude of characteristic frequency is relatively small, typical 30~40dB lower than that of the fundamental power supply frequency. Second, the characteristic frequency $(1 - 2s)f_s$ is very close the power supply frequency f_s . Under steady operating condition, the frequency distance between the characteristic frequency and the fundamental frequency f_s can be as small as $0.01f_s$. It is generally difficult to distinguish the characteristic frequency from the fundamental frequency using the traditional Fourier spectral analysis. Although a big extension of measurement time may be helpful, it requires near constant load to ensure both the slip and motor current remain stable during the whole measurement period, otherwise the load fluctuation will interfere the accuracy of fault detection. This constant load requirement in many cases can be troublesome because the unavoidable load fluctuation in reality especially over a long measurement period. Therefore, it is necessary to develop a high frequency resolution analysis method using very short time measurements to meet the real situations in BRB detection.

In the past decades, researchers have developed different MCSA methods such as Fourier transform spectral analysis, short-time Fourier transform Bellini et al. (2001); Zhao and Lipo (1996); Toliyat and Lipo (1995) and subsequent high resolution spectral analysis using ESPRIT Xu et al. (2012) and MUSIC Kim et al. (2013). Although existing methods can achieve high resolution in BRB detection,

¹ Initial work was done while Dingguo Lu was an intern with Mitsubishi Electric Research Laboratories, 201 Broadway, Cambridge, MA 02139, USA.

they have several limits. First, they still require seconds of measurements under constant load. Any load fluctuation within the measurement period could interfere the accuracy of fault detection. Second, they are not capable of detecting early-stage fault, of which the characteristic frequency component is very weak.

In recent years, the development of compressive sensing (CS) provides us a feasible solution to analyze high resolution frequency components even with few measurements. Compressive sensing is an innovative method to capture and represent sparse or compressible signals at a rate well below its Nyquist sampling rate Baraniuk (2007); Candès and Wakin (2008). This sampling rate reduction is achieved by measuring uncorrelated or randomized projections of the sparse signals and reconstructing the sparse signal using improved signal models and non-linear reconstruction algorithms. In spectral analysis this sampling rate reduction means with a fewer amount of measurements, we are able to reconstruct the same resolution frequency spectrum, or with the same amount of measurements but higher resolution than the traditional methods. In MCSA based fault detection, the motor current spectrum with fault characteristic frequency exhibits sparse characteristics in the frequency domain. Therefore, the characteristic frequency component can be resolved with high resolution using compressive sensing based techniques. Considering the fact that the characteristic frequency is distributed in the *continuous* frequency domain, we consider the off-the-grid compressive sensing technique Tang et al. (2013).

In order to verify our method, we build a dynamic model using multi-loop equivalent circuit to simulate stator current, in which a broken bar fault is modeled by an open circuit while an early stage broken-bar fault is simulated using an increased resistance of the fault branch. We then develop an off-the-grid compressive sensing algorithm to extract the characteristic frequency component in the simulated stator current.

This paper is organized as follows. In Section 2, we describe the dynamic model of induction machine for stator current simulation under healthy and fault conditions. In Section 3, we introduce compressive sensing fundamentals and our off-the-grid compressive sensing algorithm. Fault detection results on simulated data are presented in Section 4. Finally, we draw conclusions in Section 5.

2. DYNAMIC MODEL OF INDUCTION MOTOR

In squirrel-cage induction motors, the stator consists of three sinusoidally distributed windings, displaced by 120° spatial angle. The rotor contains longitudinal conductive bars connected at both ends by shorting rings, forming a squirrel-cage like shape. As the induction motor is operating, the stator windings set up a rotating magnetic field through the rotor, inducing electrical current in the rotor bars, producing force acting at a tangent orthogonal to the rotor, and resulting in torque to turn the shaft.

In the following part of this section, we first develop a dynamic model for motors in normal healthy condition, then extend it to fault conditions. For simplicity, we

neglect magnetic saturation and assume linear magnetic characteristics.

The equivalent circuit of squirrel-cage induction motor is shown in Fig.1. Assuming there are n rotor bars, the squirrel-cage rotor can then be modeled as $n + 1$ independent current loops, where n of them are identical circuit loops under ideal condition, with each loop consisting of two adjacent rotor bars connected by two end ring portions. The remaining circuit loop is formed by one of the end rings. So, the current distribution in rotor can be specified in terms of $(n + 1)$ independent loop currents, *i.e.*, n rotor-bar loop currents i_j ($1 \leq j \leq n$) plus one end ring loop current i_e .

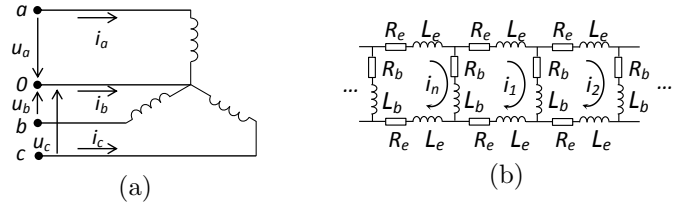


Fig. 1. Equivalent circuit of (a) stator windings, and (b) rotor in squirrel-cage induction motor

2.1 Stator Voltage and Flux Equations

Based on the equivalent circuit, the voltage and flux linkage equations for the stator windings can be written as:

$$\mathbf{U}_s = \mathbf{R}_s \mathbf{I}_s + \frac{d\mathbf{\Psi}_s}{dt}, \quad (1)$$

$$\mathbf{\Psi}_s = \mathbf{L}_s \mathbf{I}_s + \mathbf{M}_{sr} \mathbf{I}_r, \quad (2)$$

where the stator voltage

$$\mathbf{U}_s = [u_a \ u_b \ u_c]^T, \quad (3)$$

with

$$u_a = U_0 \cos(2\pi f_s t + \phi_0), \quad (4)$$

the stator current

$$\mathbf{I}_s = [i_a \ i_b \ i_c]^T, \quad (5)$$

the stator winding flux

$$\mathbf{\Psi}_s = [\psi_a \ \psi_b \ \psi_c]^T, \quad (6)$$

the stator resistance

$$\mathbf{R}_s = \begin{bmatrix} R_s & 0 & 0 \\ 0 & R_s & 0 \\ 0 & 0 & R_s \end{bmatrix}, \quad (7)$$

the stator inductance

$$\mathbf{L}_s = \begin{bmatrix} L_s & M_{ab} & M_{ac} \\ M_{ba} & L_s & M_{bc} \\ M_{ca} & M_{cb} & L_s \end{bmatrix}, \quad (8)$$

the stator-rotor mutual inductance

$$\mathbf{M}_{sr} = \begin{bmatrix} m_{a1} & m_{a2} & \cdots & m_{an} & m_{ae} \\ m_{b1} & m_{b2} & \cdots & m_{bn} & m_{be} \\ m_{c1} & m_{c2} & \cdots & m_{cn} & m_{ce} \end{bmatrix}, \quad (9)$$

and the rotor current

$$\mathbf{I}_r = [i_1 \ i_2 \ \cdots \ i_n \ i_e]^T. \quad (10)$$

Here we use bold capital letters for matrices, regular capital letters for constant parameters and small letters for time-variant parameters. It is important to note that the stator winding resistance in (7) and the inductance of

stators in (8) are constant under our assumption, while the stator-rotor mutual inductance in (9) varies with the angular position of rotor. This is because the mutual inductance is related to the relative position between the stator windings and the rotor bars, which changes during operation.

2.2 Rotor Voltage and Flux Equations

The voltage and flux linkage equations for the rotor loops can be written as:

$$\mathbf{U}_r = \mathbf{R}_r \mathbf{I}_r + \frac{d\boldsymbol{\Psi}_r}{dt}, \quad (11)$$

$$\boldsymbol{\Psi}_r = \mathbf{L}_r \mathbf{I}_r + \mathbf{M}_{rs} \mathbf{I}_s, \quad (12)$$

where the rotor voltage

$$\mathbf{U}_r = [u_1 \ u_2 \ \cdots \ u_n \ u_e]^T = [\mathbf{0}]_{(n+1) \times 1}, \quad (13)$$

the rotor flux

$$\boldsymbol{\Psi}_r = [\psi_1 \ \psi_2 \ \cdots \ \psi_n \ \psi_e]^T, \quad (14)$$

the rotor resistance

$$\mathbf{R}_r = \begin{bmatrix} R_0 & -R_b & 0 & \cdots & 0 & -R_b & R_e \\ -R_b & R_0 & -R_b & \ddots & 0 & 0 & R_e \\ 0 & -R_b & R_0 & \ddots & 0 & 0 & R_e \\ \vdots & \ddots & \ddots & \ddots & \vdots & \vdots & \vdots \\ 0 & 0 & 0 & \cdots & R_0 & -R_b & R_e \\ -R_b & 0 & 0 & \cdots & -R_b & R_0 & R_e \\ R_e & R_e & R_e & \cdots & R_e & R_e & nR_e \end{bmatrix}, \quad (15)$$

with $R_0 = 2(R_b + R_e)$, the rotor inductance

$$\mathbf{L}_r = \begin{bmatrix} L_r + L_0 & M_{12} - L_b & M_{13} & \cdots & M_{1n} - L_b & L_e \\ M_{21} - L_b & L_r + L_0 & M_{23} - L_b & \ddots & M_{2n} & L_e \\ M_{31} & M_{32} - L_b & L_r + L_0 & \ddots & M_{3n} & L_e \\ \vdots & \ddots & \ddots & \ddots & \vdots & \vdots \\ M_{n1} - L_b & M_{n2} & M_{n3} & \cdots & L_r + L_0 & L_e \\ L_e & L_e & L_e & \cdots & L_e & nL_e \end{bmatrix}, \quad (16)$$

with $L_0 = 2(L_b + L_e)$, and the rotor-stator mutual inductance $\mathbf{M}_{rs} = \mathbf{M}_{sr}^T$.

2.3 Mechanical Equations

The mechanical equation of the induction motor can be expressed as:

$$T_e - T_l = J \frac{d\omega_r}{dt}, \quad (17)$$

where T_e represents the electromagnetic torque, T_l is the load, J stands for the rotor inertia, and ω_r is the angular velocity. Using the basic principle of energy conversion, the electromagnetic torque can be calculated as:

$$T_e = \mathbf{I}_s^T \frac{d\mathbf{M}_{sr}}{d\theta_r} \mathbf{I}_r. \quad (18)$$

The angular velocity can be expressed in terms of change rate of rotor's angular position θ_r as follows:

$$\omega_r = \frac{d\theta_r}{dt}. \quad (19)$$

In summary, equations (1) ~ (19) form a dynamic model of induction motors with unknown stator and rotor currents. Given the motor parameters, we can use standard methods

for solving differential equations to simulate the stator current during dynamic operation. In this paper, we use the fourth-order Runge-Kutta method Butcher (1987).

2.4 Motor Parameters

Under normal healthy condition, the inductances and resistances in (7), (8), (9), (15) and (16) can be calculated Luo et al. (1993); Boucherma et al. (2006). To save the space of this paper, we skip the details of parameter calculations.

When one bar is fully broken, the related branch becomes open circuit. Then the totally number of circuit loops is reduced by one since the related two loops are replaced by a new loop with doubled end-ring segments, as shown in Fig. 2(a). Consequently, in (11)~(16) the corresponding loops should be removed or rebuilt with the equivalent parameters.

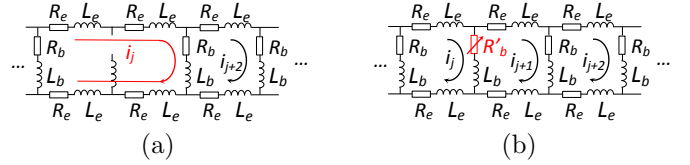


Fig. 2. Equivalent circuit of fault conditions: (a) Fully broken bar, and (b) Early-stage broken bar

If the bar is not fully broken, but in an early stage of broken fault condition, we can simulate this intermediate damage state by increasing the corresponding bar resistance to a certain value R'_b , as shown in Fig. 2(b). The more severe the damage, the larger the resistance R'_b . As a result, the related entries in our model should be modified. For example, if the bar shared by the j^{th} and the $(j+1)^{th}$ loops is damaged, then the corresponding resistance sub-block $\mathbf{R}_{r_{j,(j+1)}} = [R_0, -R_b; -R_b, R_0]$ in (15) should be modified to $[R_0 - R_b + R'_b, -R'_b; -R'_b, R_0 - R_b + R'_b]$.

Comparing to other models such as the d-q model Santos et al. (2006), this equivalent circuit model is straightforward to understand and flexible to simulate intermediate fault state. It is important to note that this model may become ill-conditioned when the ratio between R'_b and R_b is too large. A small step size inversely proportional to the ratio in the fourth-order Runge-Kutta method is then necessary for proper simulation results.

3. COMPRESSIVE SENSING BASED DETECTION

3.1 Background of Compressive Sensing

In the Shannon/Nyquist sampling theorem, the sampling rate (the so-called Nyquist rate) should be at least twice the signal bandwidth in order to exactly recover the original signal. Compressive sensing is an innovative method to capture and represent sparse or compressible signals at the rate well below Nyquist rate Candès and Wakin (2008); Baraniuk (2007). This sampling rate reduction is achieved by using uncorrelated projection measurements, improved signal models, and non-linear reconstruction algorithms. Assume the signal under observation \mathbf{x} can be represented by a sparse coefficient vector α with basis \mathbf{A} as $\mathbf{x} = \mathbf{A}\alpha$.

Measurements are made on \mathbf{x} through a projection matrix Φ as follows

$$\mathbf{y} = \Phi \mathbf{x} = \Phi \mathbf{A} \alpha = \Sigma \alpha. \quad (20)$$

According to the CS theory, if Σ satisfies the restricted isometry property, α can be reconstructed with overwhelming probability close to 1 by solving an L_1 -minimization problem Candès and Wakin (2008)

$$\min \|\alpha\|_1 \quad \text{s.t. } \mathbf{y} = \Sigma \alpha. \quad (21)$$

In order to apply the CS theory to real applications, researchers typically adopt a discretization procedure to reduce the continuous parameter space to a finite set of grid points. This strategy generally yields state-of-the-art performance for problems where the true parameters lie on the grid. However, in cases where the true parameters do not fall into the finite grid, the signal cannot often sparsely be represented by the discrete basis. In this situation, off-the-grid compressive sensing provides us a solution by generalizing the discrete basis to a continuous one Tang et al. (2013).

Suppose we observe the signal

$$x_j = \sum_{k=1}^K c_k e^{i2\pi f_k j}, \quad j \in \{0, \dots, n-1\}, \quad (22)$$

with unknown K ($K \ll n$) frequencies $f_1, \dots, f_K \in [0, 1]$ on an index set $\{j\}$ of size m ($K < m \leq n$) selected uniformly at random.

Let Δ_f be the minimum wrap-around distance of frequencies on the unit circle

$$\Delta_f = \min_{k \neq j} |f_k - f_j|. \quad (23)$$

If $\Delta_f \geq \frac{4}{(n-1)}$, there exists a constant c_μ such that

$$m \geq c_\mu \max \left\{ \log^2 \frac{n}{\delta}, K \log \frac{K}{\delta} \log \frac{n}{\delta} \right\} \quad (24)$$

is sufficient to guarantee that we can recover \mathbf{x} and localize the frequencies with probability at least $1 - \delta$ with respect to the random samples and signs. Further numerical simulations suggest that, although without theoretical support, the separable frequency distance can be as small as $\frac{1}{n}$ Tang et al. (2013). The signal recovery process is realized by solving an atomic-norm minimization problem

$$\min_{\mathbf{x}} g(\mathbf{x}) := \frac{1}{2} \|\mathbf{y} - \Phi \mathbf{x}\|_2^2 \quad \text{s.t.} \quad \|\mathbf{x}\|_{\mathbf{A}} \leq c, \quad (25)$$

where \mathbf{y} corresponds to observed noisy measurements, c is a constant bound and the atomic norm $\|\mathbf{x}\|_{\mathbf{A}}$ under the set of atoms $\mathbf{A} = \{e^{i2\pi f t + \phi}\}$ is defined as

$$\|\mathbf{x}\|_{\mathbf{A}} := \inf \left\{ \sum_{\mathbf{a} \in \mathbf{A}} c_{\mathbf{a}} : \mathbf{x} = \sum_{\mathbf{a} \in \mathbf{A}} c_{\mathbf{a}} \mathbf{a}, c_{\mathbf{a}} \geq 0 \right\}. \quad (26)$$

In our BRB fault detection problem, suppose the frequencies w_k lie in $[-W, W]$, and stator current $x(t)$ is a continuous signal of the form

$$x(t) := i_a(t) = \sum_{k=1}^K c_k e^{i2\pi w_k t}. \quad (27)$$

By taking regularly spaced Nyquist samples at $t \in \{0, 1/2W, \dots, (n-1)/2W\}$, we observe

$$x_j = \sum_{k=1}^K c_k e^{i2\pi \frac{w_k}{2W} j} = \sum_{k=1}^K c_k e^{i2\pi f_k j}, \quad (28)$$

with $f_k = \frac{w_k}{2W} \in [-\frac{1}{2}, \frac{1}{2}]$, which is exactly the same as (22) after a trivial translation of the frequency domain.

With off-the-grid compressive sensing, we are able to perform fault detection by extracting sparse characteristic frequency component in the stator current signal with improved performance.

3.2 Off-the-Grid Compressive Sensing Algorithm

There are several reconstruction algorithms to reconstruct the sparse signal, with different computational complexity and accuracy Tang et al. (2013); Rao et al. (2013). These algorithms minimize a least-square loss function that measures the difference between the signal representation and the observations, subject to a constraint in terms of an atomic norm as in (25). In general, it takes long time for those algorithms to converge to the extract sparse frequency. In our fault detection applications, since we have some prior knowledge about the frequency distribution, i.e., the characteristic frequency, if there exists any, should be close to the fundamental frequency, we can predefine the atoms for fast reconstruction. For example, the stator current consists fundamental power supply frequency and possible fault characteristic frequency which is close to the power supply frequency. In our simulation, we refine frequency grid in the neighborhood of the fundamental frequency with neighborhood radius 5Hz while only consider coarse grid elsewhere. Based on this idea, we propose a conditional gradient method with predefined atoms for efficient reconstruction.

The algorithm is summarized as follows.

Algorithm 1 Condition gradient with predefined atoms

- (1) **Input:** Measurements \mathbf{y} , predefined \mathbf{A} , estimated bound c , frequency tolerance ϵ ;
 - (2) **Initialize:** $\mathbf{a}_0 \in \mathbf{A}$, $\tau \leftarrow 0$, $\mathbf{A}_0 \leftarrow [\mathbf{a}_0]$, $\mathbf{c}_0 \leftarrow [c]$, $\mathbf{x}_0 \leftarrow [\mathbf{A}_0 \mathbf{c}_0]$;
 - (3) **REPEAT**
 $\mathbf{a}_{\tau+1} \leftarrow \arg \min_{\mathbf{a} \in \mathbf{A}} \langle \nabla g(\mathbf{x}_\tau), \mathbf{a} \rangle$; **{FORWARD}**
 $\hat{\mathbf{A}}_{\tau+1} \leftarrow [\mathbf{A}_\tau \mathbf{a}_{\tau+1}]$;
 $\gamma_{\tau+1} \leftarrow \arg \min_{\gamma \in [0,1]} g[\mathbf{x}_\tau + \gamma(\hat{\mathbf{A}}_{\tau+1} \mathbf{c}_{\tau+1} - \mathbf{x}_\tau)]$;
{LINE SEARCH}
 $\tilde{\mathbf{c}}_{\tau+1} \leftarrow [(1 - \gamma_{\tau+1})\mathbf{c}_\tau; \gamma_{\tau+1}]$;
Merge adjacent frequencies within ϵ
 - (4) **UNTIL convergence**
 - (5) **Output:** \mathbf{c}_τ , \mathbf{A}_τ ;
-

4. SIMULATION

4.1 Algorithm Validation

To examine our algorithm, we consider a noise free signal represented as follows:

$$x(t) = 1.0 \cos(2\pi 50t + \phi_1) + 0.1 \cos(2\pi 150t + \phi_3) + 0.01 \cos(2\pi 48.62t + \phi_2). \quad (29)$$

As we can see, the signal is composed of three frequency components: a fundamental power supply frequency component at 50 Hz with a unit magnitude, a third harmonic

frequency component with 1/10 unit magnitude and a characteristic fault frequency component at 48.62 Hz with 1/100 unit magnitude. The initial phases are randomly chosen from $[0, 2\pi)$. The Fourier frequency spectrum is shown in the upper part of Fig. 3 where we measure 0.7 second current signal with sampling rate of 1kHz. Because of the leakage of fundamental frequency energy, it is not feasible to detect the fault characteristic frequency component using the traditional Fourier transform method since the frequency component is very close to the fundamental frequency and its magnitude is too low. When we use off-the-grid compressive sensing technique on the same 0.7 second signal, we reconstruct all three components exactly, in both magnitude and frequency, as shown in the lower part of Fig. 3. This result agrees with the aforementioned off-the-grid theory in Section 3.

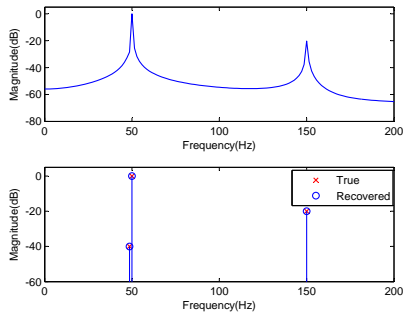


Fig. 3. Fourier spectrum (upper) and CS reconstruction (lower)

4.2 Off-the-Grid CS Based Fault Detection

To further test our method, we simulate the stator current under both healthy condition and fault condition using our multi-loop circuit model. The model parameters are extracted from a 1.5kW three-phase squirrel-cage induction motor with parameters listed in Table 1.

Table 1. Motor parameters

n	f_s (Hz)	R_s (Ω)	R_e ($\mu\Omega$)	R_b ($\mu\Omega$)
29	50	3.43	37	133.4
L_s (H)	L_r (mH)	L_b (μ H)	L_e (μ H)	J ($kg \cdot m^2$)
0.51563	5.443	1.08	0.01	0.0014

Under healthy condition, the simulated stator current of phase-A and the rotor speed are shown in Fig. 4. We notice that after about 0.5 second transient operation, the motor runs in a steady state with a constant speed.

For fault condition, we consider three different situations: two consecutive broken bars, one broken bar and one early-stage broken bar. For fully broken bar situations, we employ the equivalent circuit model as shown in Fig.2(a). While for the early-stage broken bar, which is generally not trivial to simulate, we consider resistance $R'_b = 1000R_b$ to simulation this early fault degradation for simplicity.

We sample stator current in a period of 0.7 second when the motor is operating in a steady state, assuming in practice the fluctuated load can be treated as unchanged in such a short time. Considering measurement noise in

real applications, we add noise of 30dB SNR into the simulated current signal. We then employ both the traditional Fourier transform and our off-the-grid compressive sensing method to reconstruct the sparse frequency components of stator current signals under both healthy and fault conditions, with the results plotted in Fig. 5 for comparison. The top-row figures, from left to right, show the state currents of healthy, two-broken bar, one-broken bar, and one early-stage broken bar conditions, respectively. The middle-row figures show the corresponding Fourier spectra and the bottom-row figures show the off-the-grid CS reconstruction. As we can see, the characteristic frequency components of all the three fault conditions are extracted successfully, even when the magnitude is about 40dB lower than the fundamental frequency component and the traditional Fourier spectrum fails. As regarding to the computational time, our it takes about 2.5 seconds for our off-the-grid CS algorithm to reconstruct the signal on a 3.6GHz Intel Xeon CPU using Matlab.

While we take a closer look at the sparse characteristic frequency, we observe that under the same load condition, the characteristic frequencies are slightly different, which are 47.575Hz, 47.675Hz, and 48.125Hz for two-broken bar, one-broken bar, and one early-stage broken bar conditions respectively. This interesting observation indicates that there is a possibility to diagnose the severity of the fault conditions using the high resolution off-the-grid CS analysis. The closer to the power supply frequency, the less severe the fault. This is however under investigation in our future work.

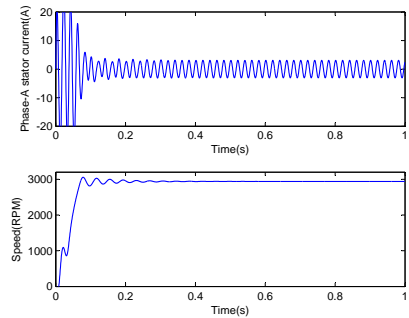


Fig. 4. Stator current (upper) and rotor speed (lower) under healthy condition

5. CONCLUSION

In this paper, we propose to use off-the-grid compressive sensing technique to detect broken bar fault in squirrel-cage induction motor. Simulation results show that due to its high frequency resolution, off-the-grid compressive sensing can effectively detect broken-bar faults, even early stage broken-bar faults with very short time measurements. In our future work, tests on experimental data will be considered for detecting and diagnosing broken-bar fault in squirrel cage induction motors.

REFERENCES

- Baraniuk, R.G. (2007). Compressive sensing [lecture notes]. *IEEE Signal Processing Magazine*, 24(4), 118–121.

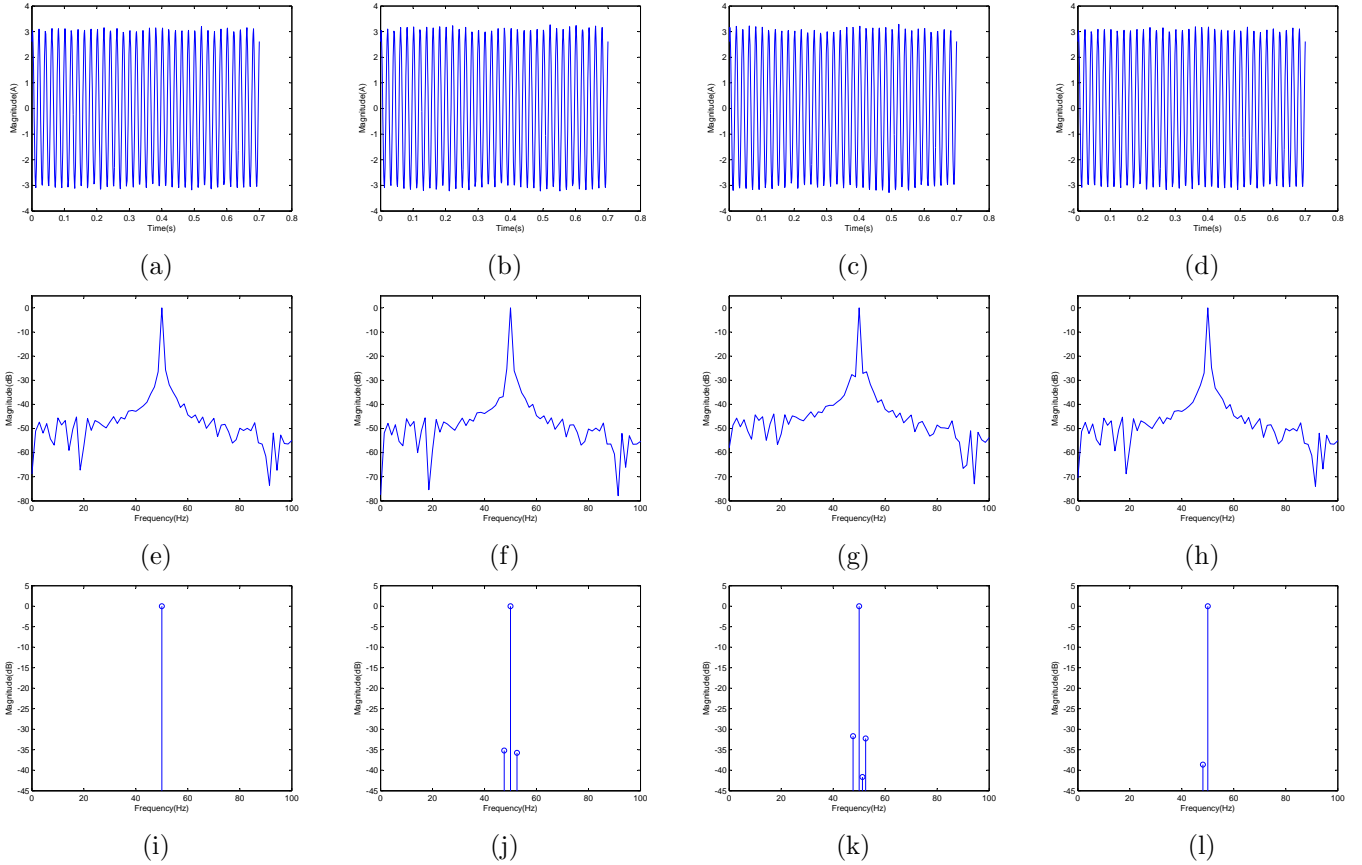


Fig. 5. (a)-(d) Stator current under healthy, two-broken-bar fault, one-broken-bar fault, and one partial-broken-bar fault respectively, (e)-(h) Fourier spectrum of (a)-(d), (i)-(l) off-the-grid CS reconstruction of (a)-(d).

Bellini, A., Filippetti, F., Franceschini, G., Tassoni, C., and Kliman, G.B. (2001). Quantitative evaluation of induction motor broken bars by means of electrical signature analysis. *IEEE Transactions on Industry Applications*, 37(5), 1248–1255.

Boucherma, M., Kaikaa, M.Y., and Khezzer, A. (2006). Park model of squirrel cage induction machine including space harmonics effects. *Journal of Electrical Engineering*, 57(4), 193 – 199.

Butcher, J.C. (1987). *The numerical analysis of ordinary differential equations: Runge-Kutta and general linear methods*. Wiley-Interscience.

Candès, E.J. and Wakin, M.B. (2008). An introduction to compressive sampling. *IEEE Signal Processing Magazine*, 25(2), 21–30.

Filippetti, F., Franceschini, G., Tassoni, C., and Vas, P. (1998). AI techniques in induction machines diagnosis including the speed ripple effect. *IEEE Transactions on Industry Applications*, 34(1), 98–108.

Kim, Y., Youn, Y., Hwang, D., Sun, J., and Kang, D. (2013). High-resolution parameter estimation method to identify broken rotor bar faults in induction motors. *IEEE Transactions on Industrial Electronics*, 60(9), 4103–4117.

Luo, X., Liao, Y., Toliyat, H., El-Antably, A., and Lipo, T.A. (1993). Multiple coupled circuit modeling of induction machines. In *Conference Record of the 1993 IEEE Industry Applications Society Annual Meeting*, volume 1, 203–210.

Rao, N., Shah, P., and Wright, S. (2013). Conditional gradient with enhancement and truncation for atomic norm regularization. In *NIPS workshop on Greedy Algorithms*.

Santos, P.M., Correa, M.B.R., Jacobina, C.B., da Silva, E.R.C., Lima, A.M.N., Didiery, G., Raziky, H., and Lubiny, T. (2006). A simplified induction machine model to study rotor broken bar effects and for detection. In *Proceedings of the 37th IEEE Power Electronics Specialists Conference (PESC)*, 1–7.

Tang, G., Bhaskar, B., Shah, P., and Recht, B. (2013). Compressed sensing off the grid. *IEEE Transactions on Information Theory*, 59(11), 7465–7490.

Toliyat, H.A. and Lipo, T.A. (1995). Transient analysis of cage induction machines under stator, rotor bar and end ring faults. *IEEE Transactions on Energy Conversion*, 10(2), 241–247.

Xu, B., Sun, L., Xu, L., and Xu, G. (2012). An ESPRIT-SAA-based detection method for broken rotor bar fault in induction motors. *IEEE Transactions on Energy Conversion*, 27(3), 654–660.

Zhang, P., Du, Y., Habetler, T.G., and Lu, B. (2011). A survey of condition monitoring and protection methods for medium-voltage induction motors. *IEEE Transactions on Information Theory*, 47(1), 34–46.

Zhao, Y. and Lipo, T.A. (1996). Modeling and control of a multi-phase induction machine with structural unbalance. *IEEE Transactions on Energy Conversion*, 11(3), 570–577.